

A Brief History of Exterior Ballistics

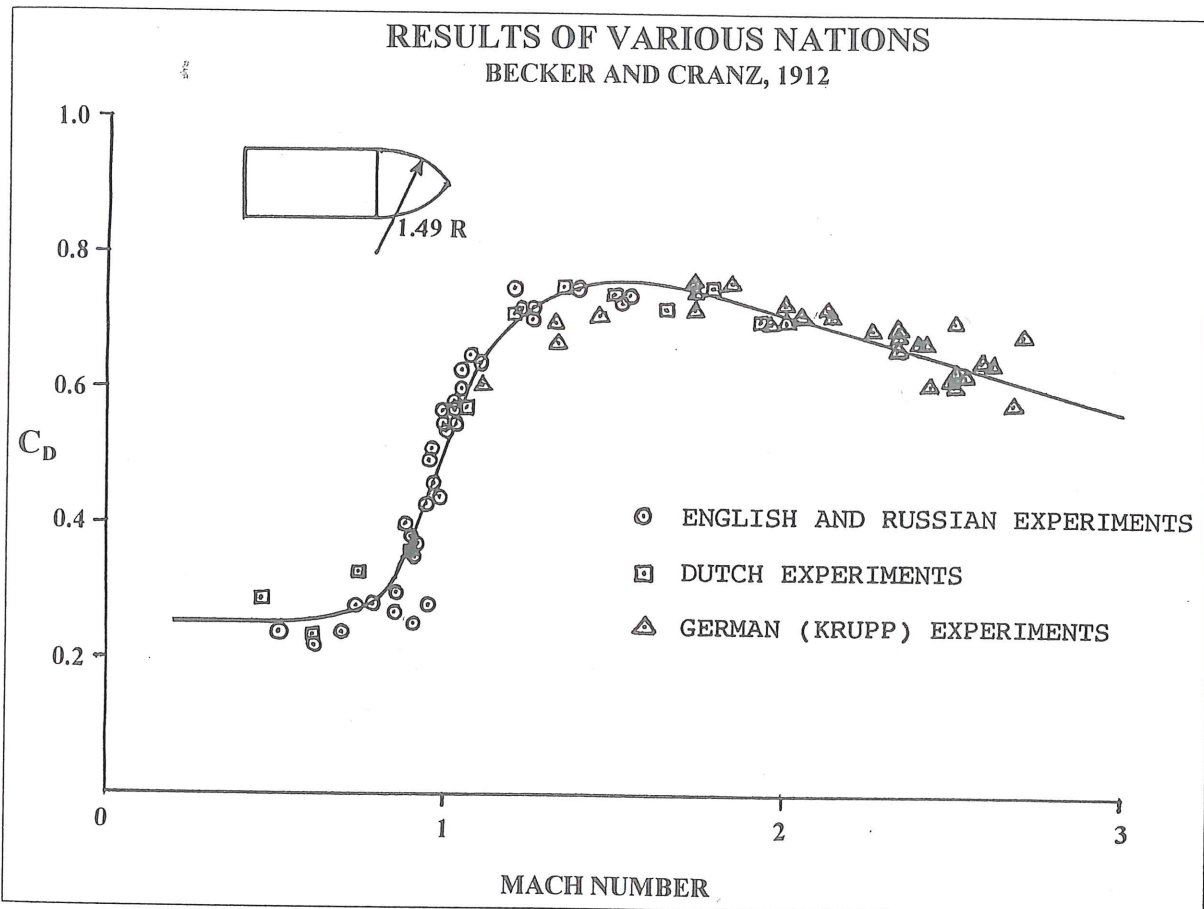
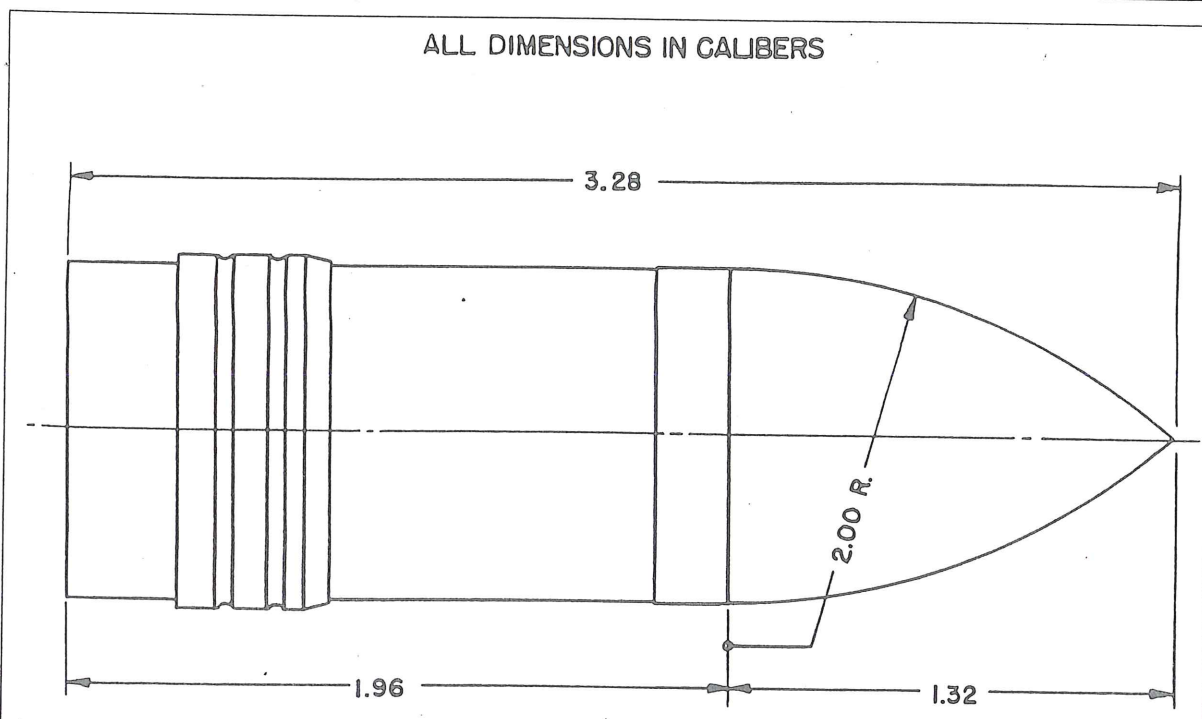


Figure 1.1 Nineteenth Century Drag Coefficients



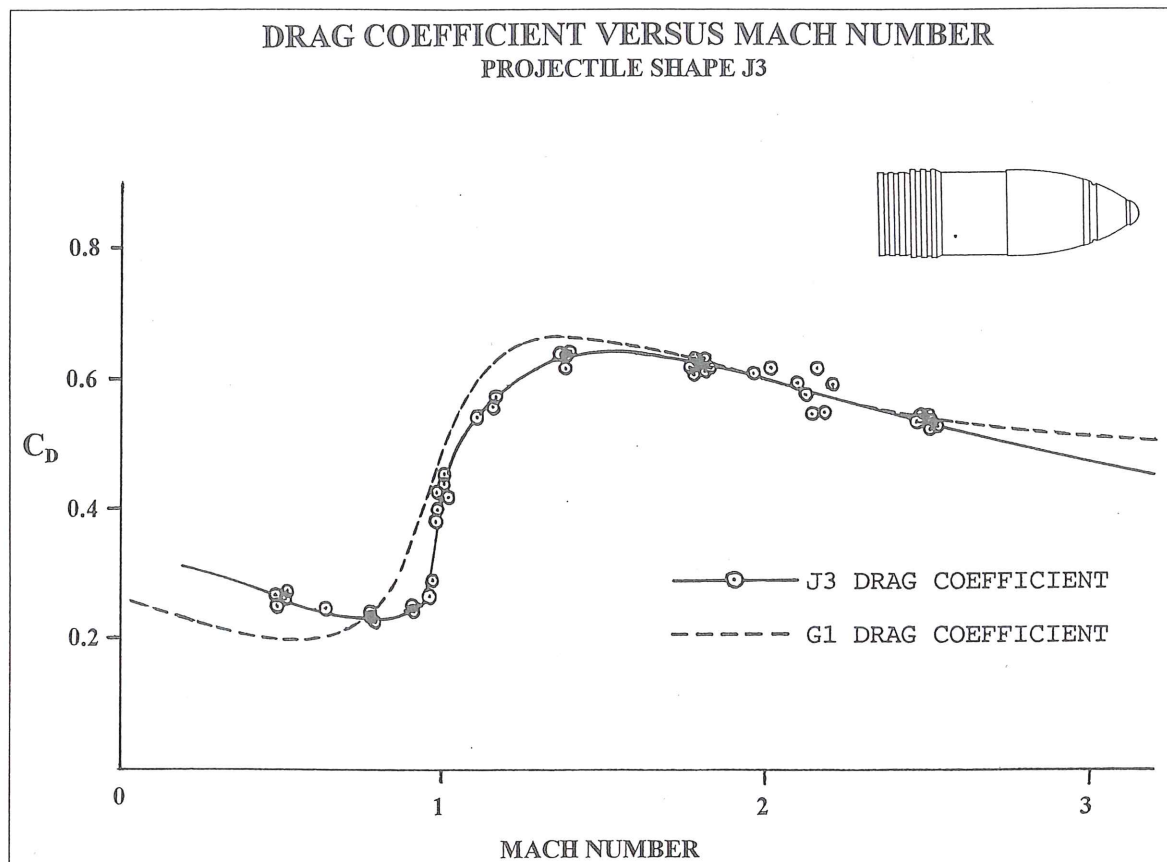


Figure 1.5 Comparison of J3 and G1 Drag Coefficients.

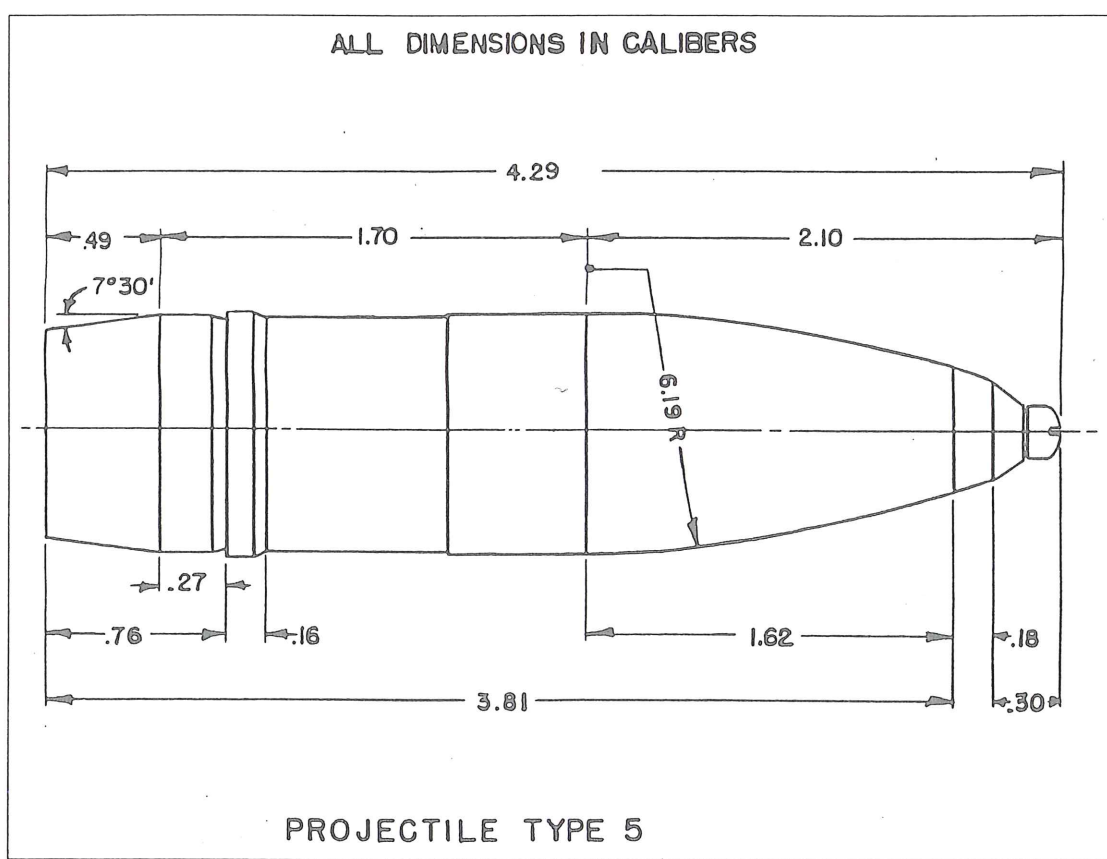


Figure 1.6 Sketch of Projectile Type 5.

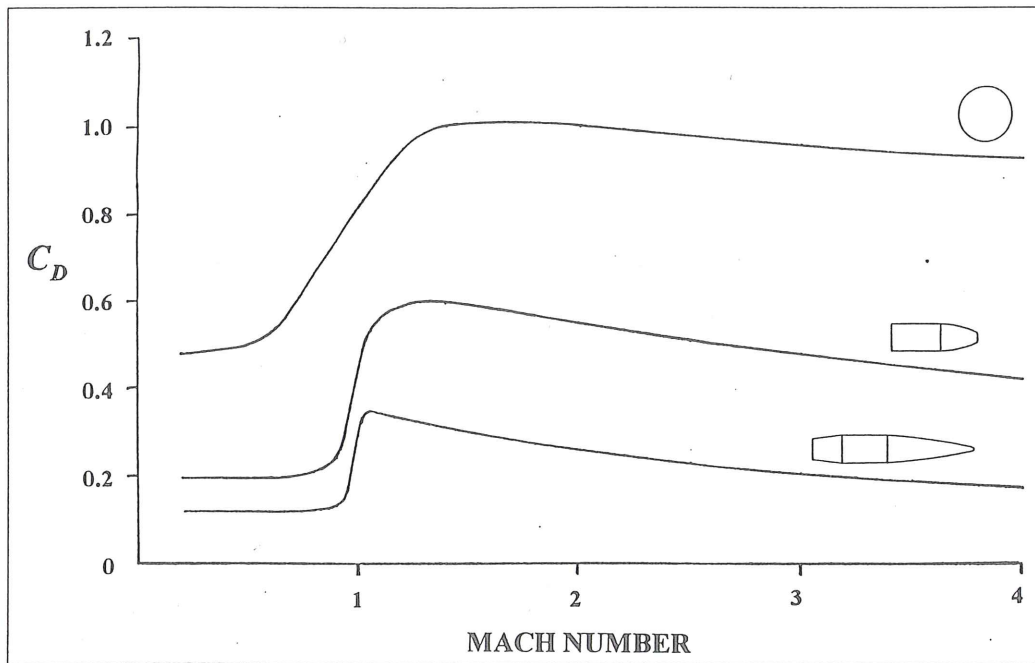


Figure 4.6 Drag Coefficients for Three Projectile Shapes.

(nose-tip flat) diameter of 0.35 caliber. This projectile has approximately twice the drag coefficient of the BRL-1 shape, at all speeds. The upper curve in Figure 4.6 is a plot of the drag coefficient versus Mach number for a 9/16 inch diameter smooth steel sphere. The sphere drag coefficient is nearly four times that of the very low drag BRL-1 shape!

The three drag coefficient plots shown in Figure 4.6 have some common characteristics. At subsonic flight speeds (Mach numbers well below 1.0), the drag coefficients are essentially constant. The drag coefficient rises sharply near Mach 1.0, then slowly decreases

at higher supersonic speeds. The sudden rise in C_D that occurs at flight speeds just below the speed of sound is caused by the formation of shock waves in the flowfield around the projectile.

The nature of subsonic, transonic and supersonic flow is clearly illustrated by a series of twelve spark shadowgraphs recently taken in the BRL Aerodynamics Range (Ref. 7) for the caliber .50 Ball M33 bullet (Ref. 8). The M33 is a typical boattailed small arms projectile, whose dimensions are shown in Figure 4.7; the measured zero-yaw drag coefficient variation with Mach number is plotted in Figure 4.8.

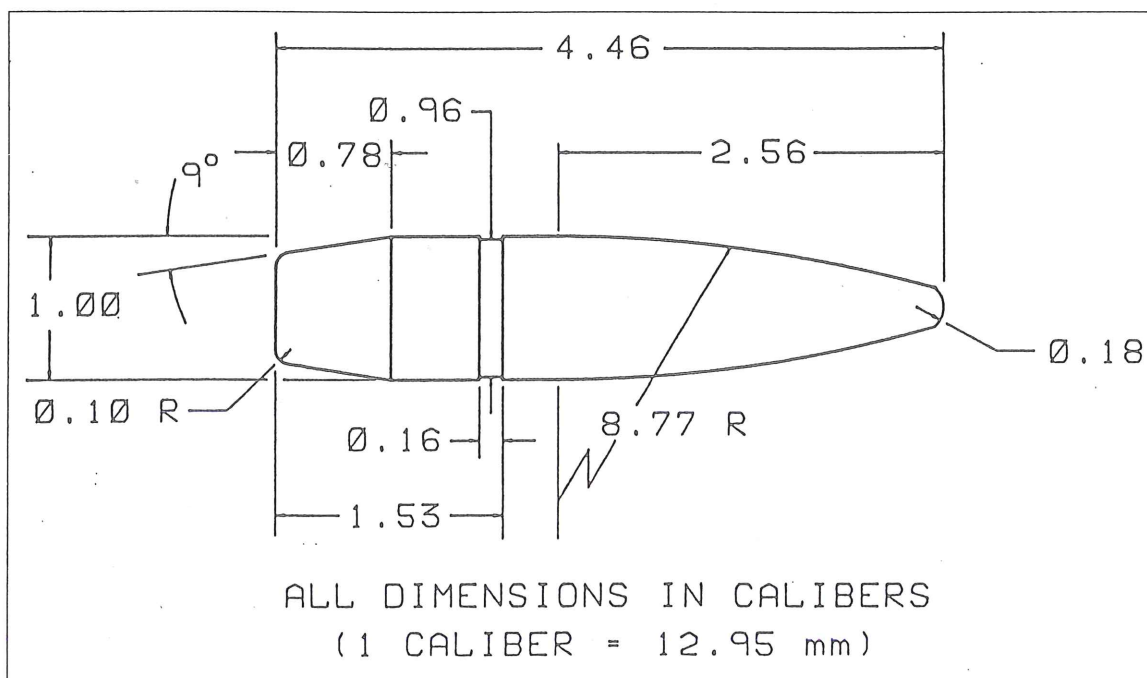


Figure 4.7 Sketch of the Caliber .50 Ball M33 Projectile.

Notes on Aerodynamic Drag

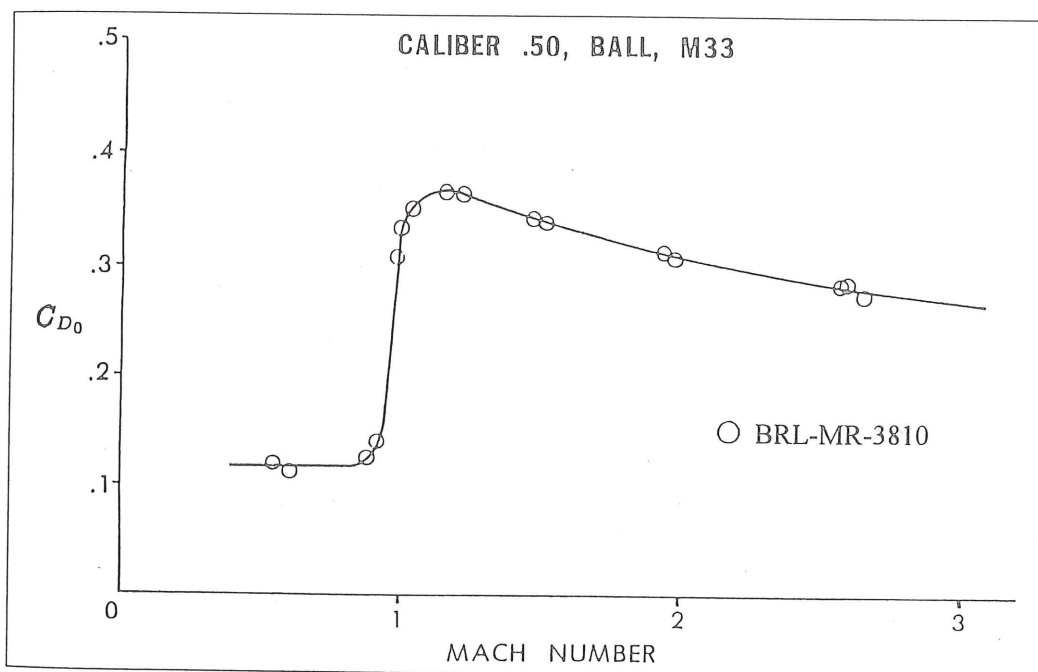
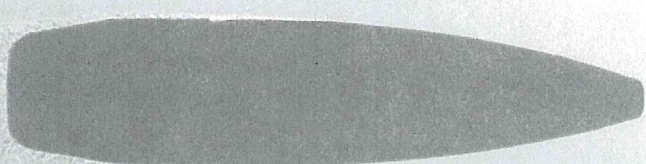


Figure 4.8 Zero-Yaw Drag Coefficient versus Mach Number for the Caliber .50 Ball M33 Projectile.



Notes on Aerodynamic Drag

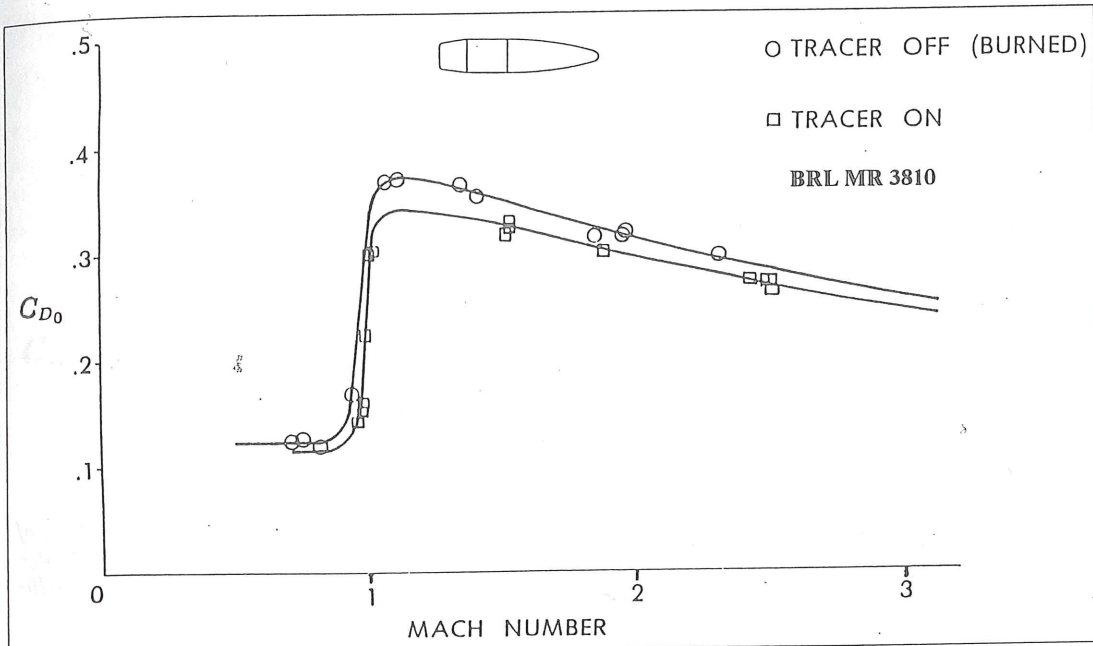


Figure 4.28 The effect of a Burning Tracer on the Drag Coefficient.

The curves of Figures 4.26 and 4.27 are relatively flat for boattail angles between five and nine degrees. The popular nine-degree boattail, which has been used for many good projectile designs, gives about two percent higher total drag than does an optimum seven-degree boattail angle. However, boattail angles steeper than ten degrees usually cause boundary layer separation, which destroys the boattail effectiveness as a drag-reducing device.

4.6 THE EFFECT OF A BURNING TRACER ON DRAG

Tracers are often used with ordnance projectiles to provide a visual trajectory indicator to the gunner. The pyrotechnic tracer mixture, which is pressed into a cavity in the projectile base, is ignited in the

barrel of the gun by the burning propellant, and the in-flight burning time of the tracer is controlled by the amount and the burning rate of the pyrotechnic mixture.

In flight, the burning tracer injects hot gas into the turbulent wake behind the projectile, which raises the base pressure and thereby lowers the drag. Since the trajectory of the tracer round is usually required to ballistically match the flight of a companion high explosive or armor piercing projectile, the exterior ballistian must know, at least approximately, how much the burning tracer reduces the drag.

Some typical effects of burning tracers on the drag of small caliber projectiles are illustrated in Figures 4.28 and 4.29. The tracer-

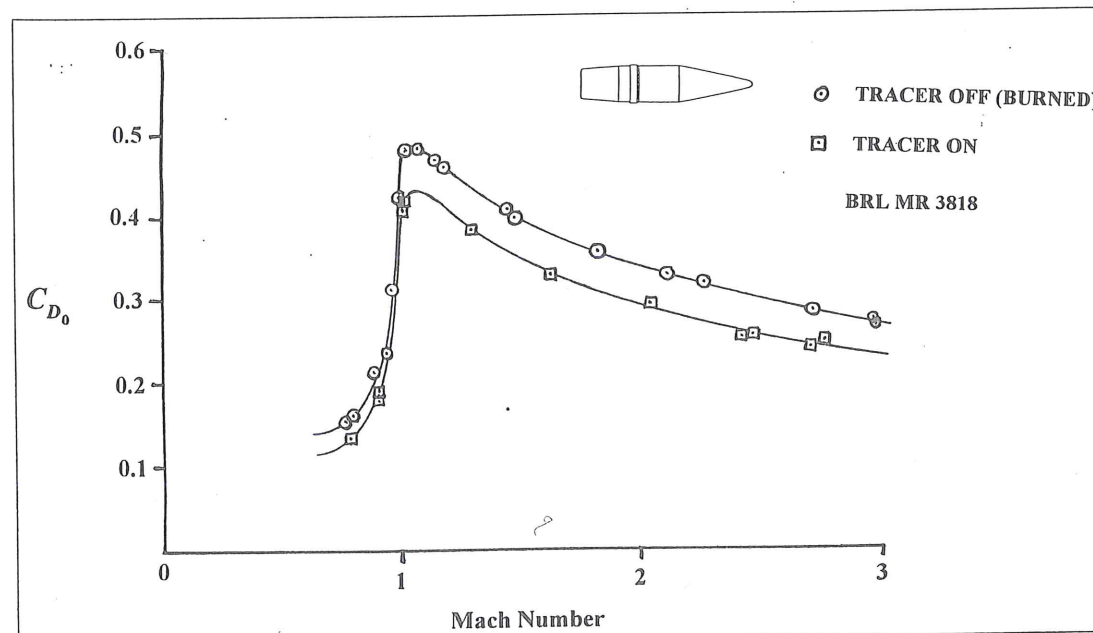


Figure 4.29 The effect of a Burning Tracer on the Drag Coefficient.

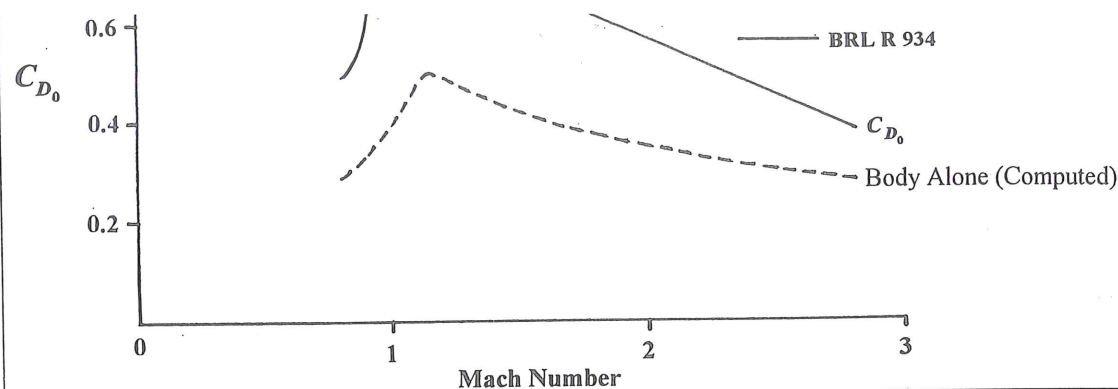


Figure 4.30 The effect of Rectangular, Single-W fin configurations on the Drag Coefficient.

drag effect is determined by firing one group of test rounds with burned-out or inert tracers, and another group of rounds with burning tracers, in a modern facility such as the BRL Aerodynamics Range. Figure 4.28 shows that the burning tracer reduces the drag of the caliber .50 APIT M20 projectile (Ref. 8) by approximately seven percent at supersonic speeds. The tracer effect on the drag coefficient of an anti-aircraft 20mm projectile is shown in Figure 4.29; this higher burning rate tracer reduces the drag by about twelve percent at supersonic speeds.

The concept of a very high burning rate tracer has evolved into the modern base-burn projectile design, in which a high energy fuel

is used instead of a pyrotechnic mixture. Drag reductions approaching thirty percent have recently been achieved with optimized base-burn configurations. It is probable that long-range artillery will be the primary future application of base-burn technology.

4.7 THE EFFECT OF FINS ON THE DRAG

Fin-stabilized projectiles are frequently employed in modern ordnance design. Mortars, flechettes, long-rod kinetic energy penetrators and rocket-powered missiles are typical examples of projectiles that are not suitable for spin stabilization. This section illustrates the experimental drag coefficients obtained for several typical finned ordnance designs.

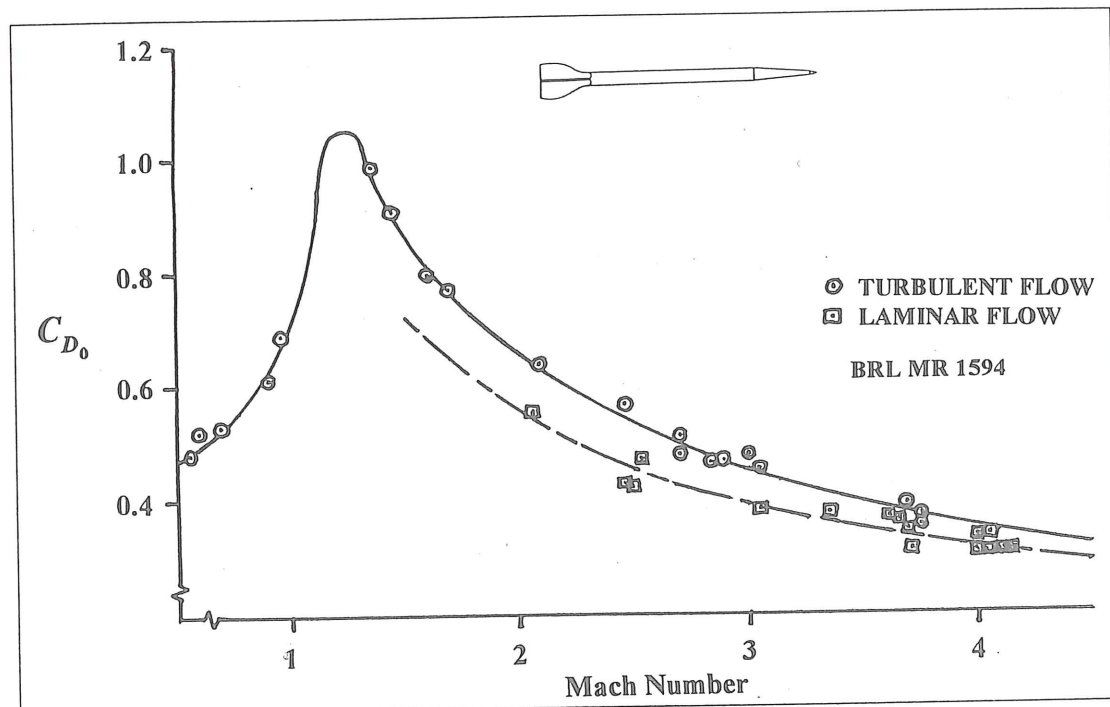


Figure 4.31 The Drag Coefficient of a Flechette with Laminar and Turbulent Boundary Layer.

Notes on Aerodynamic Drag

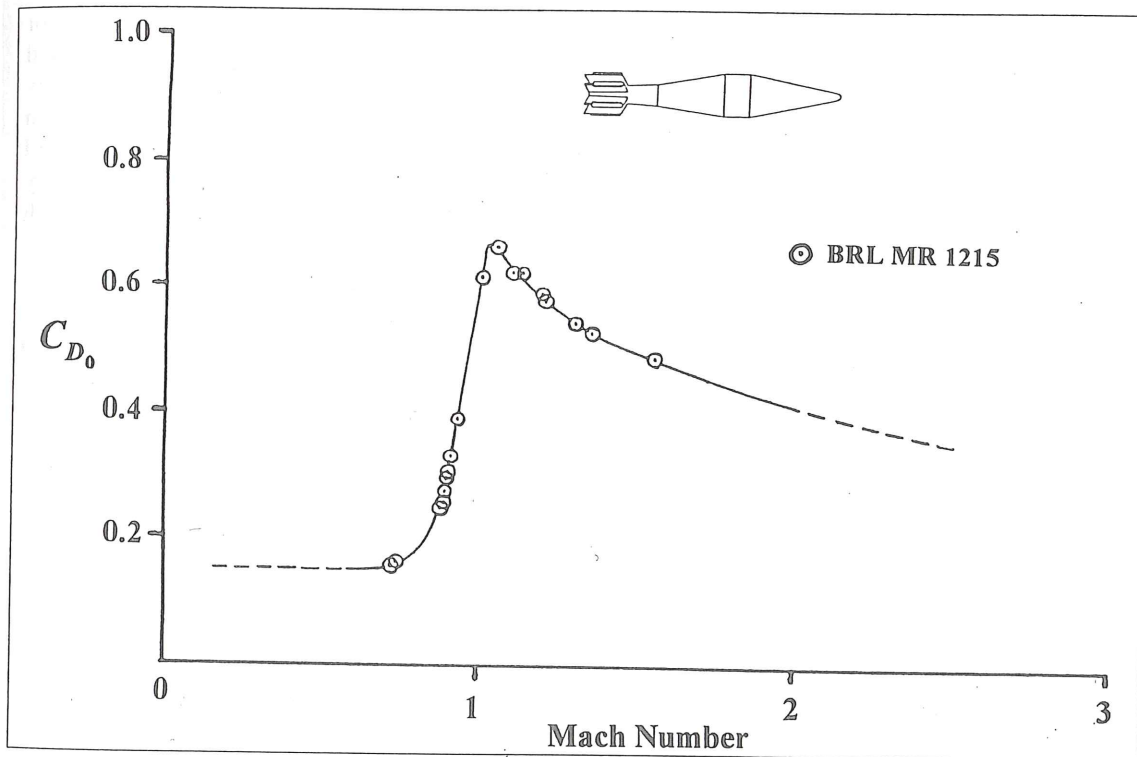


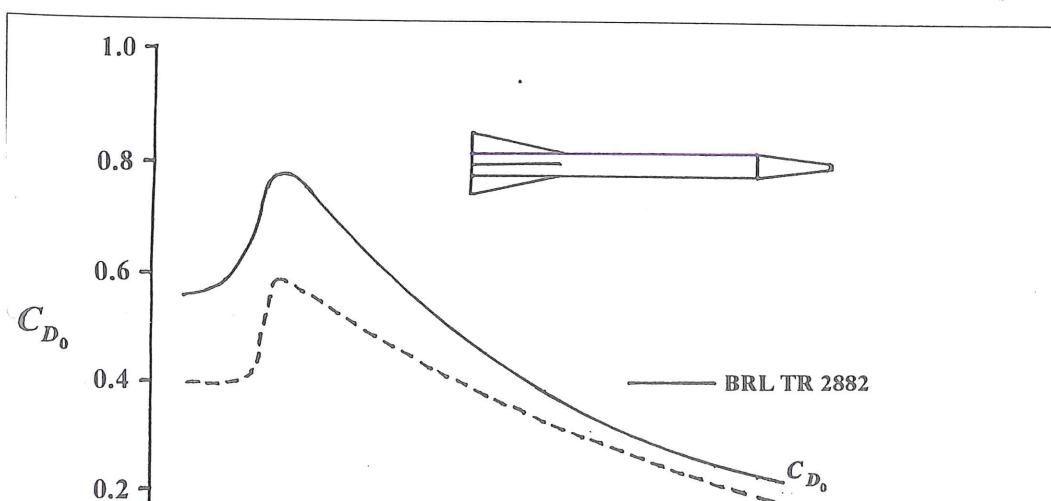
Figure 4.32 The Drag Coefficient of a Typical Fin-Stabilized Ordnance Projectile.

Figure 4.30 shows the total drag coefficient and the body-alone contribution for the 20mm Basic Finner model (Ref. 19). The Basic Finner is a ten-caliber long cone-cylinder projectile, with four square planform, single-wedge, 0.08 caliber thickness fins. Approximately forty percent of the total Basic Finner drag is due to the fins.

The drag coefficient of a ten-grain steel flechette (Ref. 6) is illustrated in Figure 4.31. The flechette has a cone-cylinder body

whose diameter is 1.79mm (0.0705 inch); the total length is 23.5 calibers. Four flat-plate fins with an average fin thickness of 0.10 caliber, and a three-caliber total span, are used to stabilize the flechette.

In section 4.3 we noted that the Reynolds number effect on drag is usually small enough to be neglected; however, the flechette of Figure 4.31 is an exception to that general rule. At flight speeds



Notes on Aerodynamic Drag

ARMY-NAVY SPINNER ROCKET

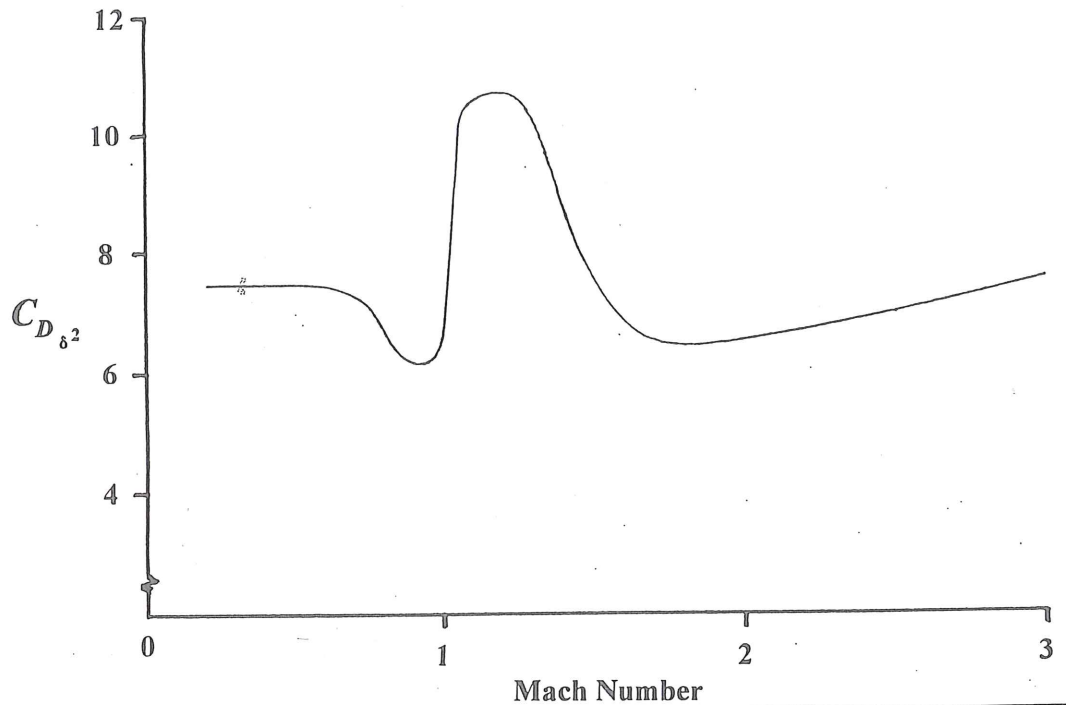


Figure 4.38 Yaw-Drag Coefficient versus Mach Number.

ARMY-NAVY SPINNER ROCKET

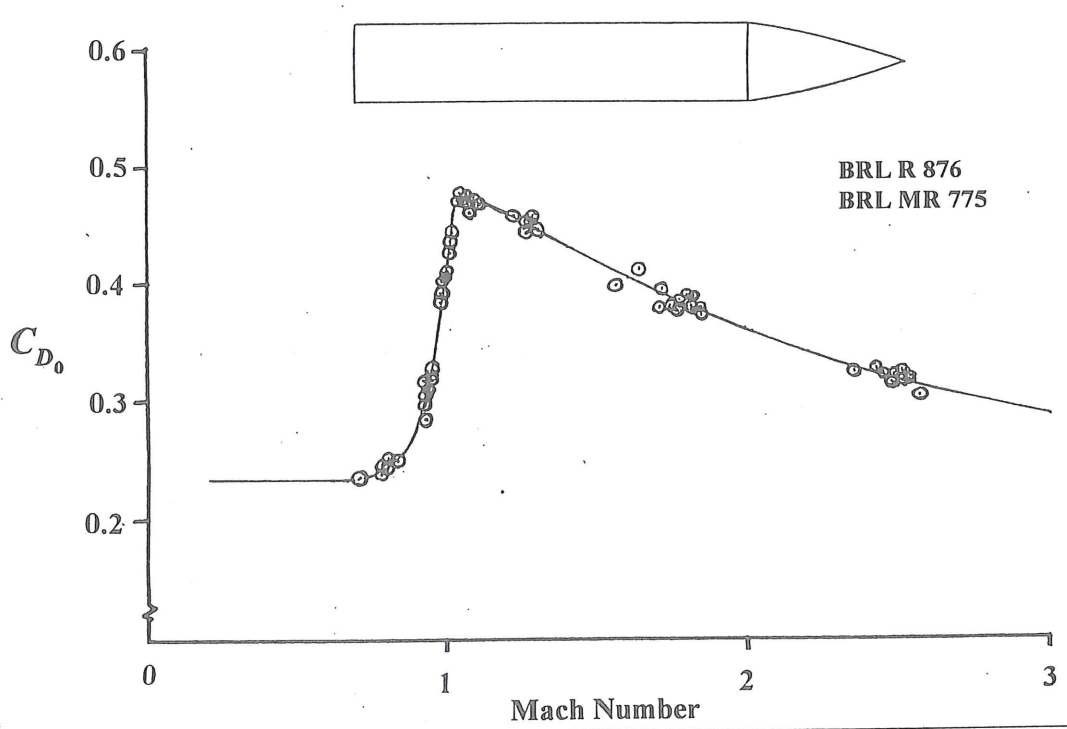


Figure 4.38 Zero-Yaw Drag Coefficient versus Mach Number.

Notes on Aerodynamic Drag

20MM CONE-CYLINDER

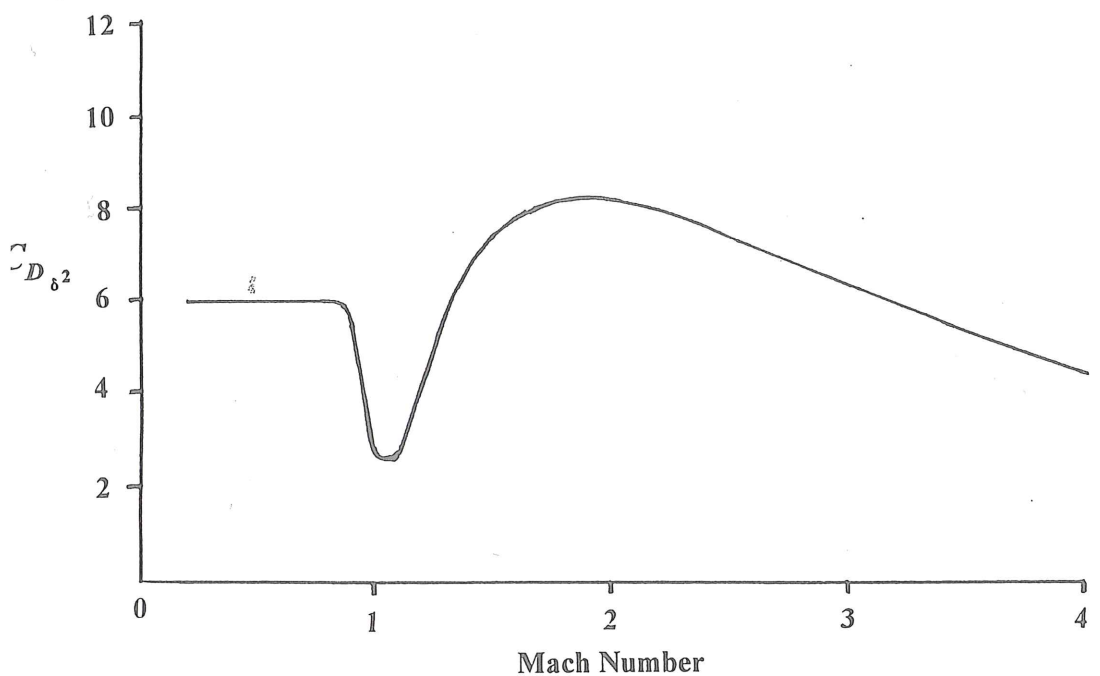


Figure 4.41 Yaw-Drag Coefficient versus Mach Number.

20MM CONE-CYLINDER

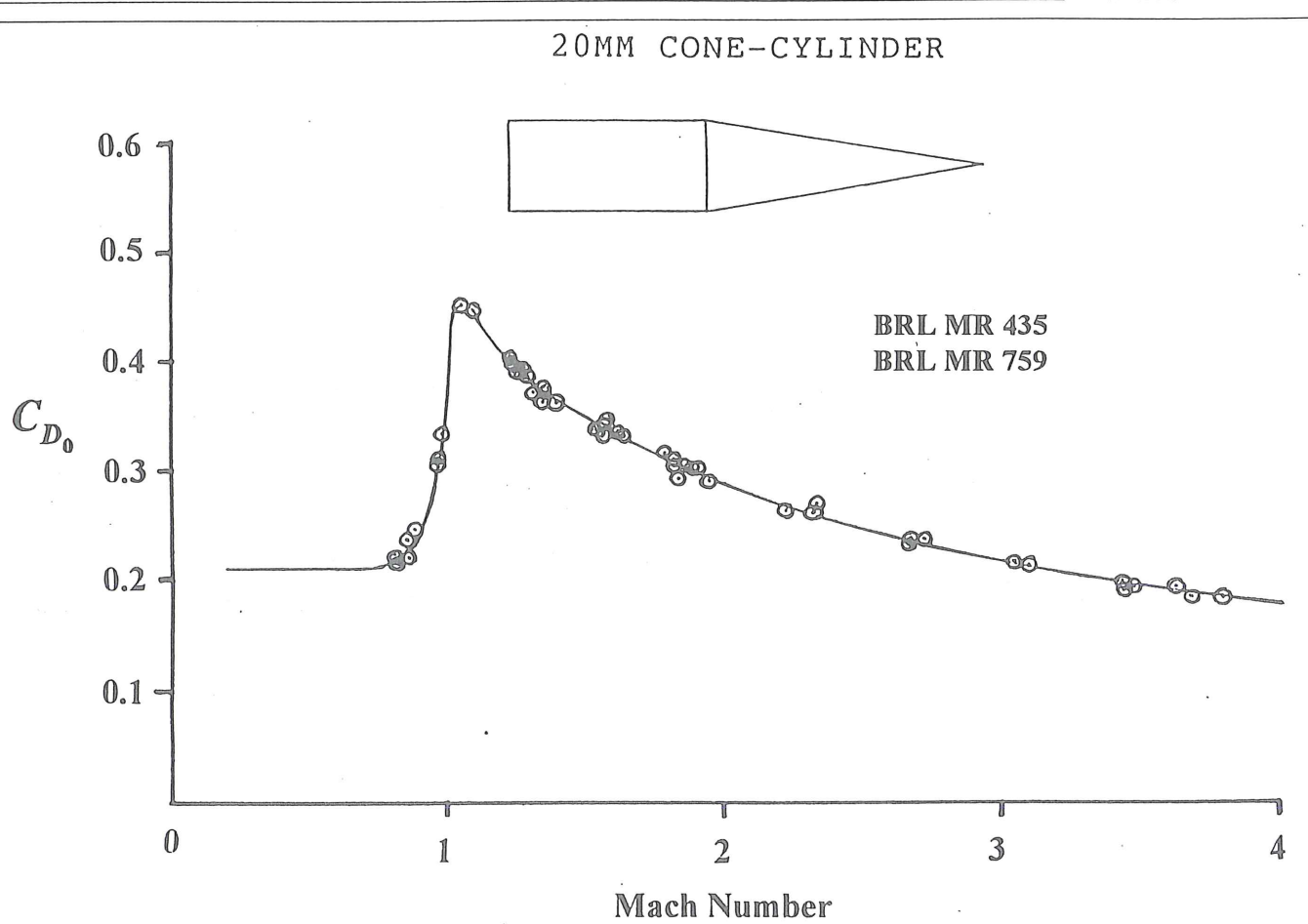


Figure 4.41 Zero Yaw Drag Coefficient versus Mach Number.

Notes on Aerodynamic Drag

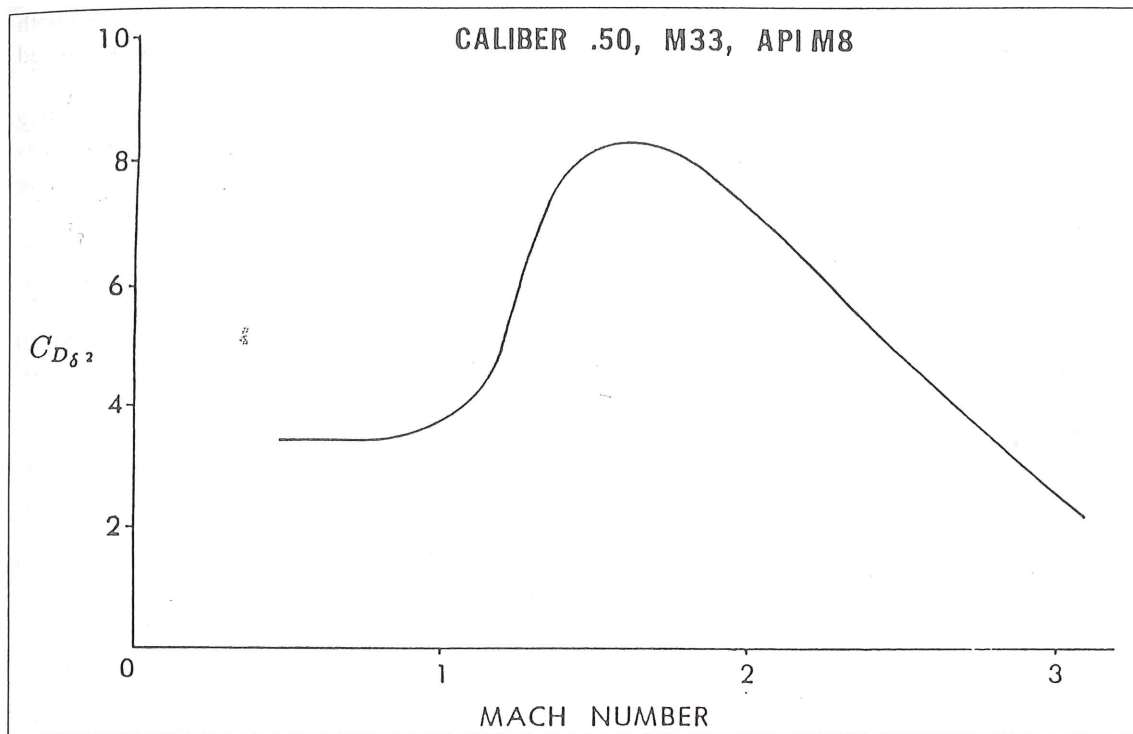


Figure 4.44 Yaw-Drag Coefficient versus Mach Number.

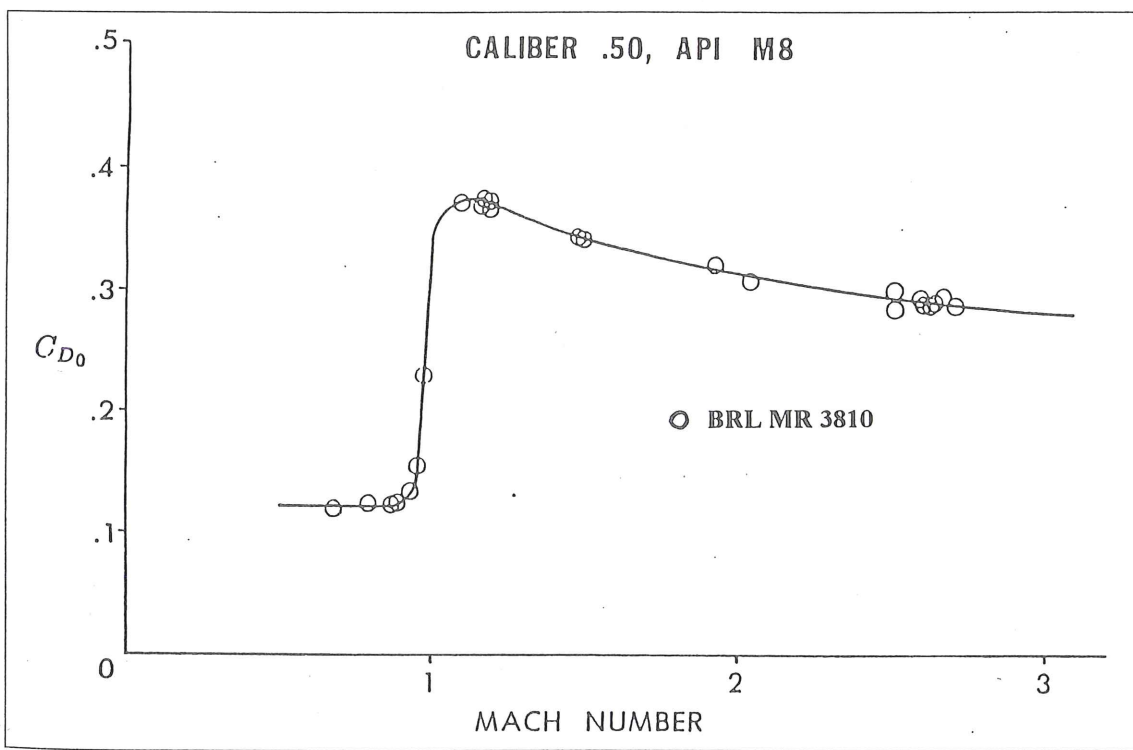


Figure 4.44 Zero Yaw Drag Coefficient versus Mach Number for the Caliber .50 API M8 Projectile.

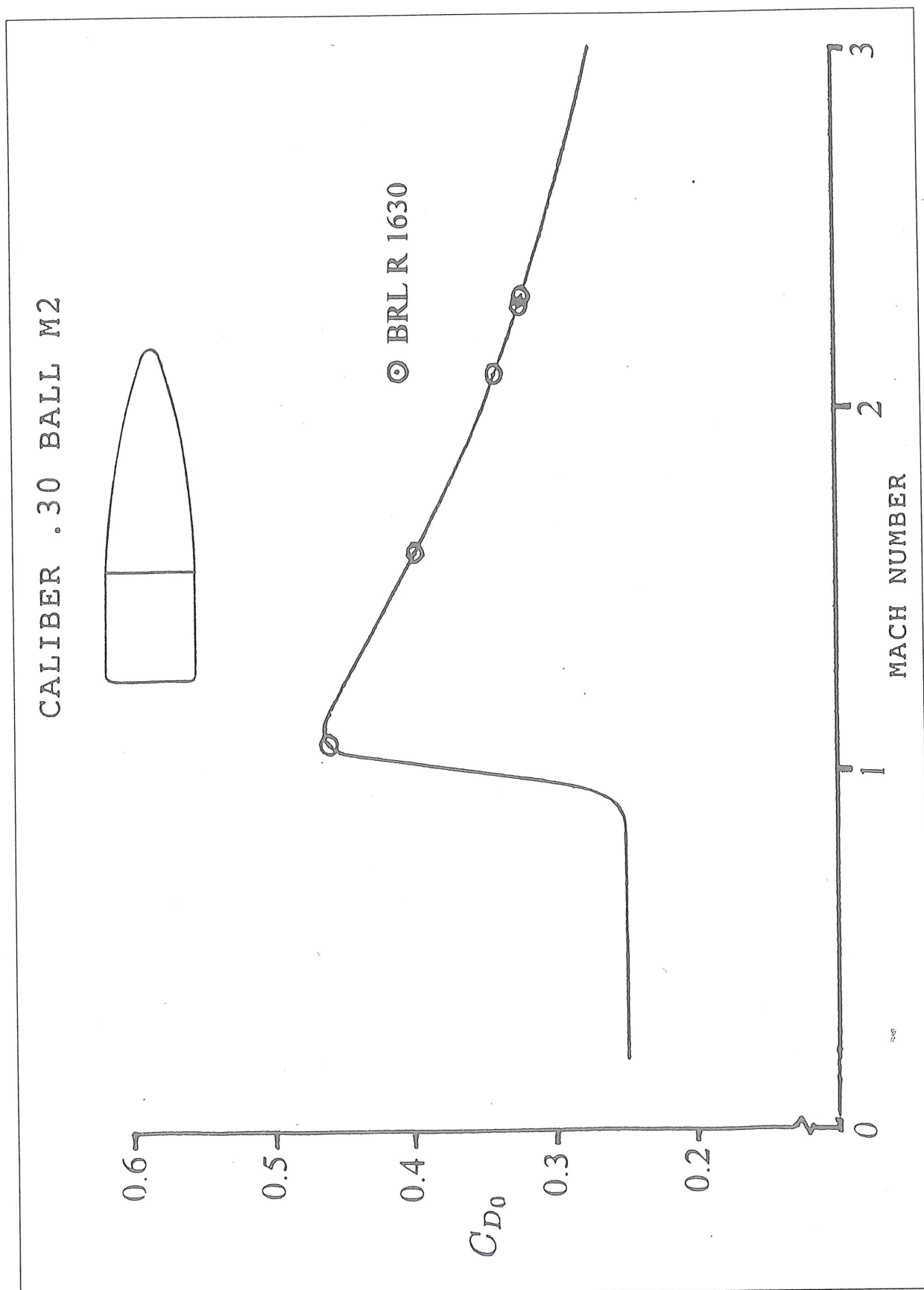


Figure 6.1 Zero-Yaw Drag Coefficient versus Mach Number.

V	2810	.112	17.6
100	2571	.234	29.8
200	2349	.368	35.8
300	2135	.516	34.1
400	1930	.680	23.0
500	1733	.863	0.3
600	1547		

The largest difference in velocity is 10 feet per second; the times of flight agree to within 0.001 second, and the largest difference in trajectory height is 0.1 inch. In general, the Siacci method agrees very well with the results of modern numerical methods.

The next example illustrates the determination of the ballistic coefficient and the form factor from a known velocity-distance table.

Example 6.3

A table of striking velocity versus range for the 7.62mm Ball M80 bullet, fired at a muzzle velocity of 2810 feet per second, is given in Table 6.7. The reference diameter is 0.308" and the nomi-

7.62mm Ball M80 - Numerical

Range (Yards)	Striking Velocity (feet per second)
0	
100	
200	
300	
400	
500	
600	

The velocities in Table 6.7 are recorded per second. The values of $S(V)$ in the G_1 , obtained for five feet per second intervals, are tabulated values. For example, $S(V)$ at $V = 1760$ fps is the tabulated $S(V)$ values at $V = 1760$ fps

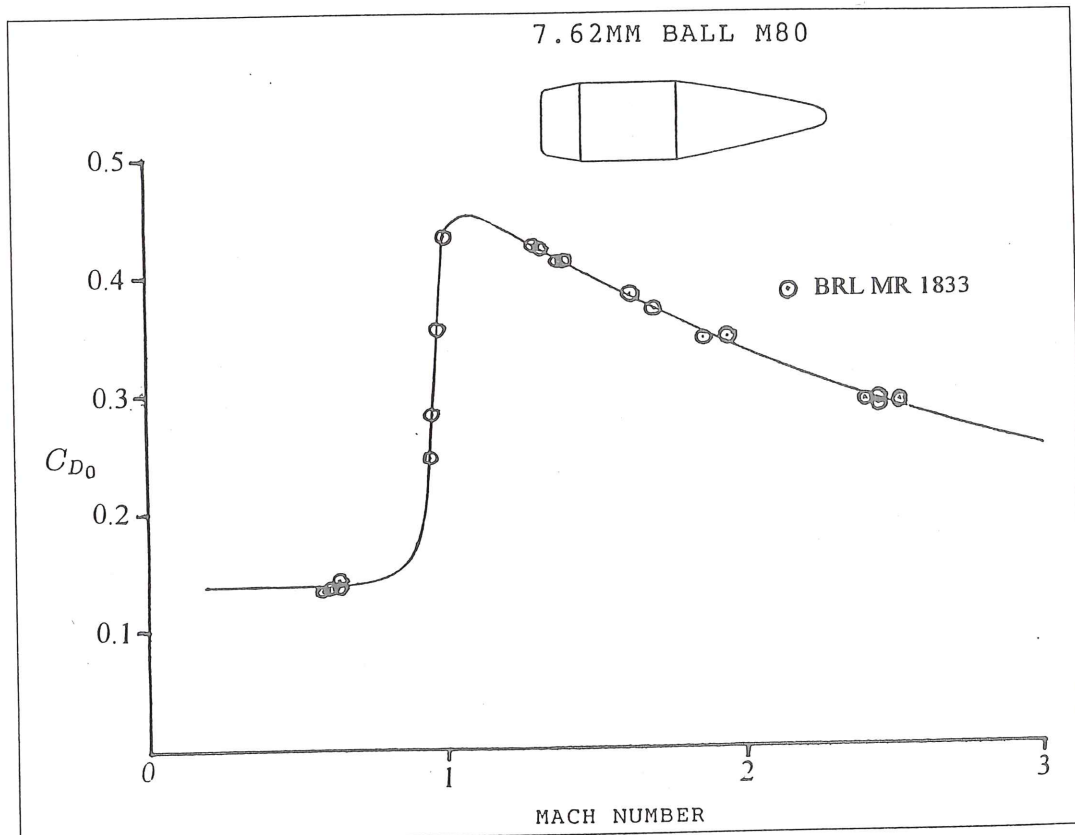


Figure 6.3
Drag coefficient

The Point-Mass Trajectory

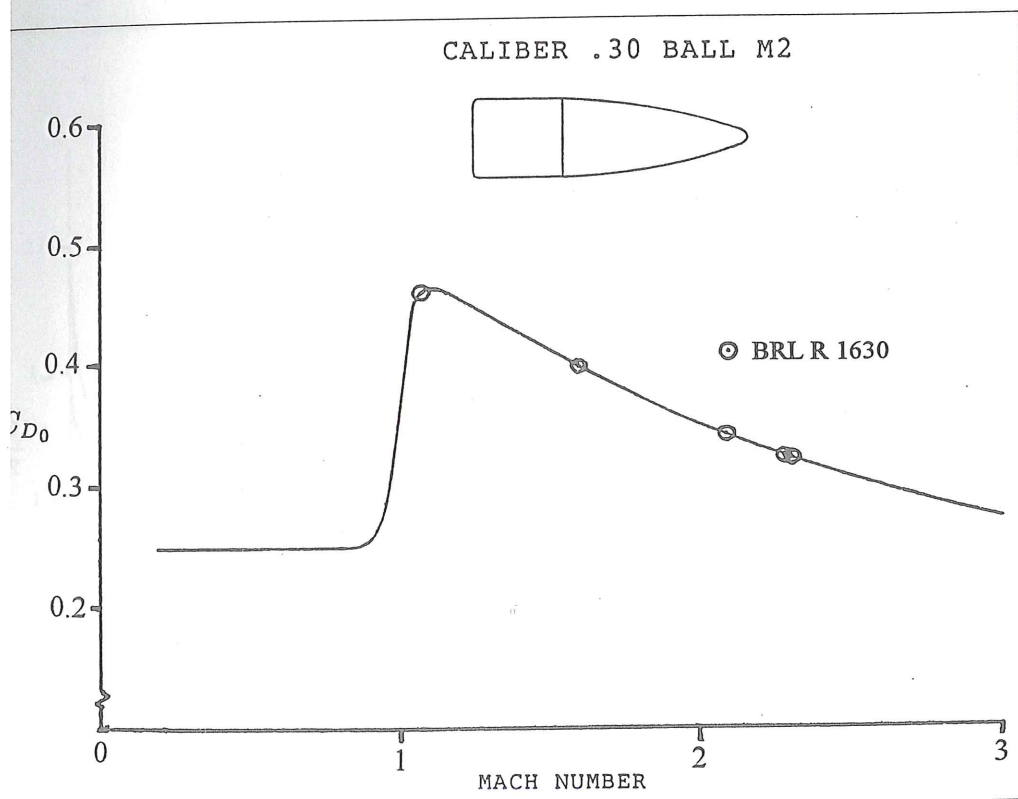


Figure 8.4 Zero-Yaw Drag Coefficient versus Mach Number.

DRAG FUNCTION: .30 BALL M2

MACH NO.	CD
0	.25
.8	.25
.9	.252
.95	.288
1	.362
1.05	.443
1.1	.464
1.2	.456
1.4	.427
1.6	.399
1.8	.373
2	.351
2.2	.331
2.5	.305
3	.271

ARMY STANDARD METRO

PROJECTILE IDENTIFICATION: .30 BALL M2

MUZ VEL (FT/SEC)	C (LB/IN ²)	H ₀ (INCHES)	ELEV (MINUTES)	DENSITY RATIO
2800	.226	0	19	1

DRAG FUNCTION: G8 DRAG FUNCTION

MACH NO.	CD
0	.211
.8	.21
.9	.211
.95	.257
1	.407
1.05	.448
1.1	.448
1.2	.435
1.4	.406
1.6	.378
1.8	.352
2	.329
2.2	.308
2.5	.28
3	.243

ARMY STANDARD METRO

PROJECTILE IDENTIFICATION: .30 BALL M2 - RUN WITH G8 DRAG FUNCTION

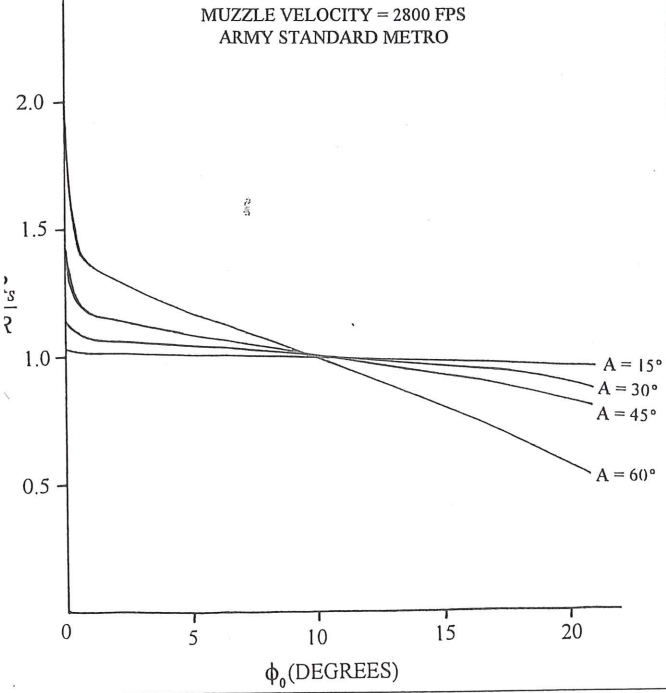
MUZ VEL (FT/SEC)	C (LB/IN ²)	H ₀ (INCHES)	ELEV (MINUTES)	DENSITY RATIO
2800	.21	0	19	1

The Point-Mass Trajectory

UPHILL FIRING

CALIBER 0.30 BALL M2

MUZZLE VELOCITY = 2800 FPS
ARMY STANDARD METRO



DOWNTHILL FIRING

CALIBER 0.30 BALL M2

MUZZLE VELOCITY = 2800 FPS
ARMY STANDARD METRO

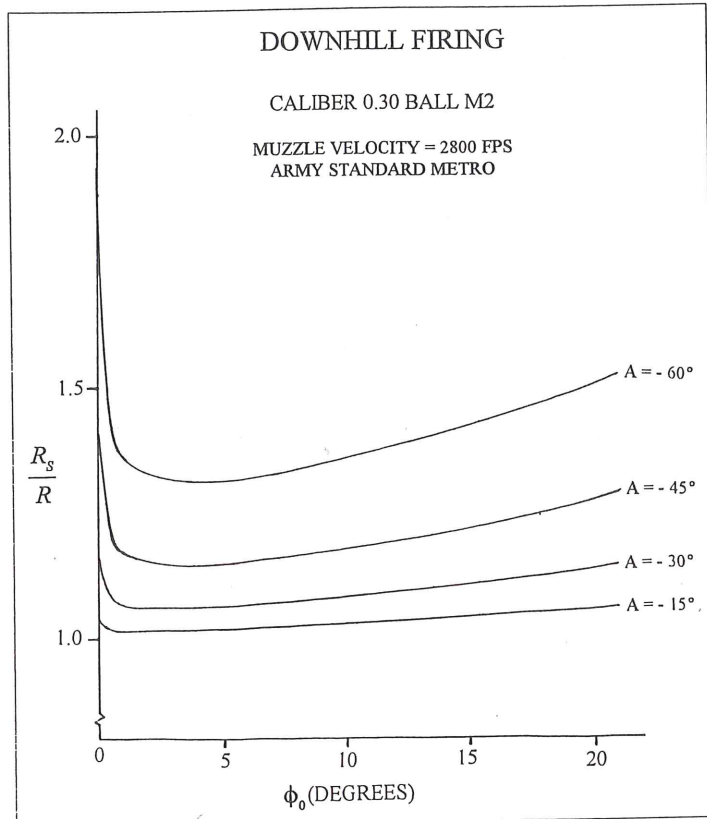


Figure 8.8 Ratio of Slant Range to Ground Range versus Gun Elevation Angle (Up hill).

Figure 8.9 Ratio of Slant Range to Ground Range versus Gun Elevation Angle (Downhill).

105 mm, M1

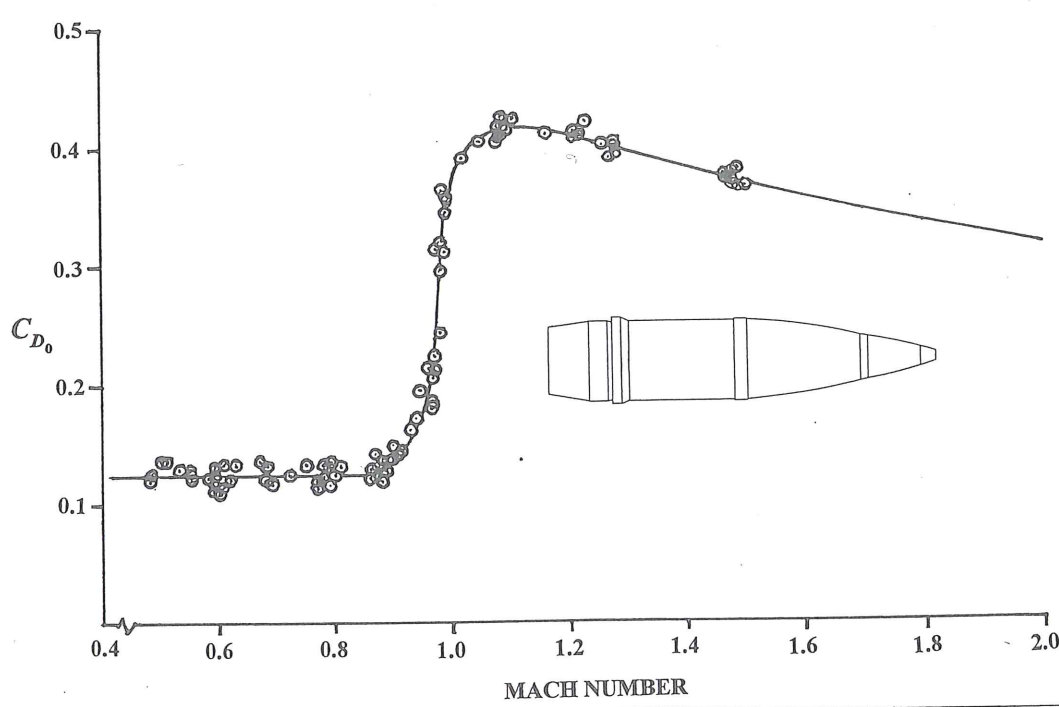


Figure 8.10 Zero-Yaw Drag Coefficient versus Mach Number; 105 mm M1 Shell.

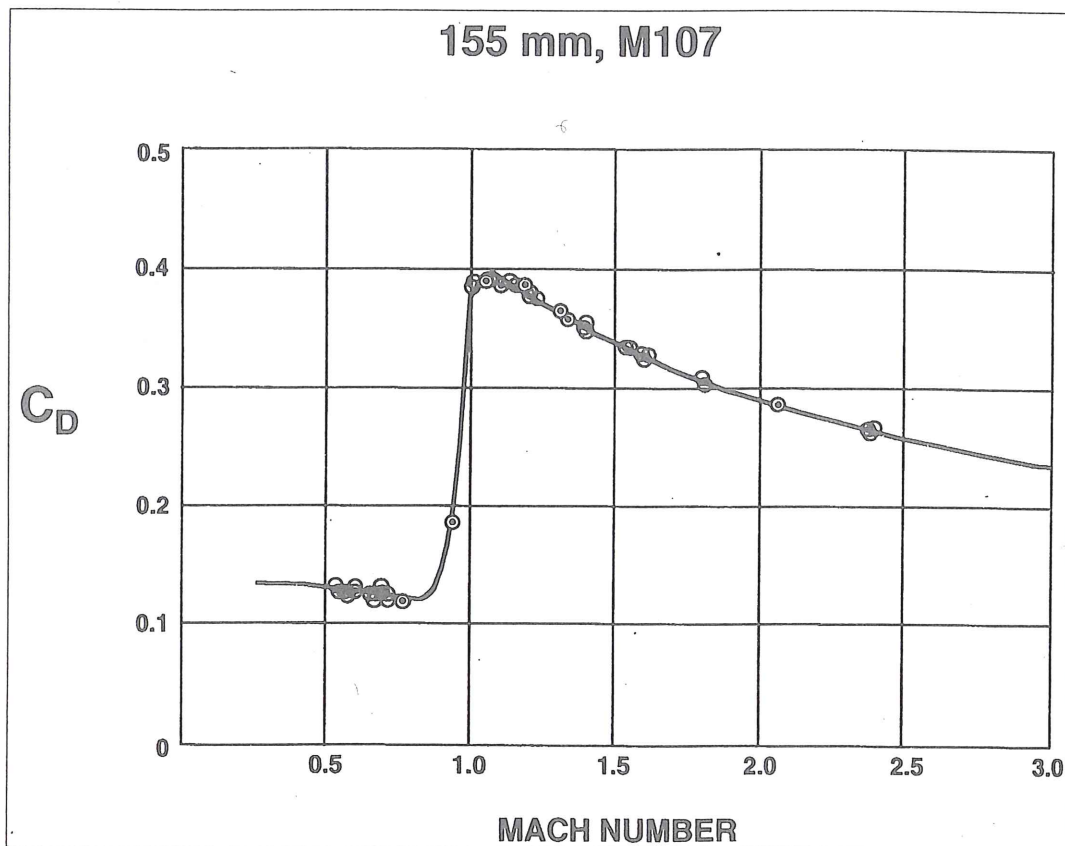


Figure 8.17
efficient versus
mm M107 S

Table 8.10
Flat-Fire Vacuum Approximations for Horizontal Coriolis Drift
7.62mm Ball M80 - Muzzle Velocity = 2810 FPS

		[Point-Mass]	[Equation 8.52]	[Equation 8.54]
Range (Yards)	$[V_x]_{AVE}$ (FPS)	Defl. (In.)	Defl. (In.)	Defl. (In.)
500	2276	0.6	0.5	0.6
1000	1819	2.8	2.0	3.1
1500	1532	7.6	4.5	8.2
2000	1364	15.9	7.9	16.3

Table 8.11
(Latitude of Firing Site = 45 Degrees, North)

[Coriolis Effect]				
Azimuth of Fire (Degrees)	Impact Range (Meters)	Impact Defl. (Meters)	-Range (Meters)	-Deflection (Meters)
0 (North)	17970	37	0	37
90 (East)	17995	56	25	56
180 (South)	17970	74	0	74
270 (West)	17945	56	-25	56

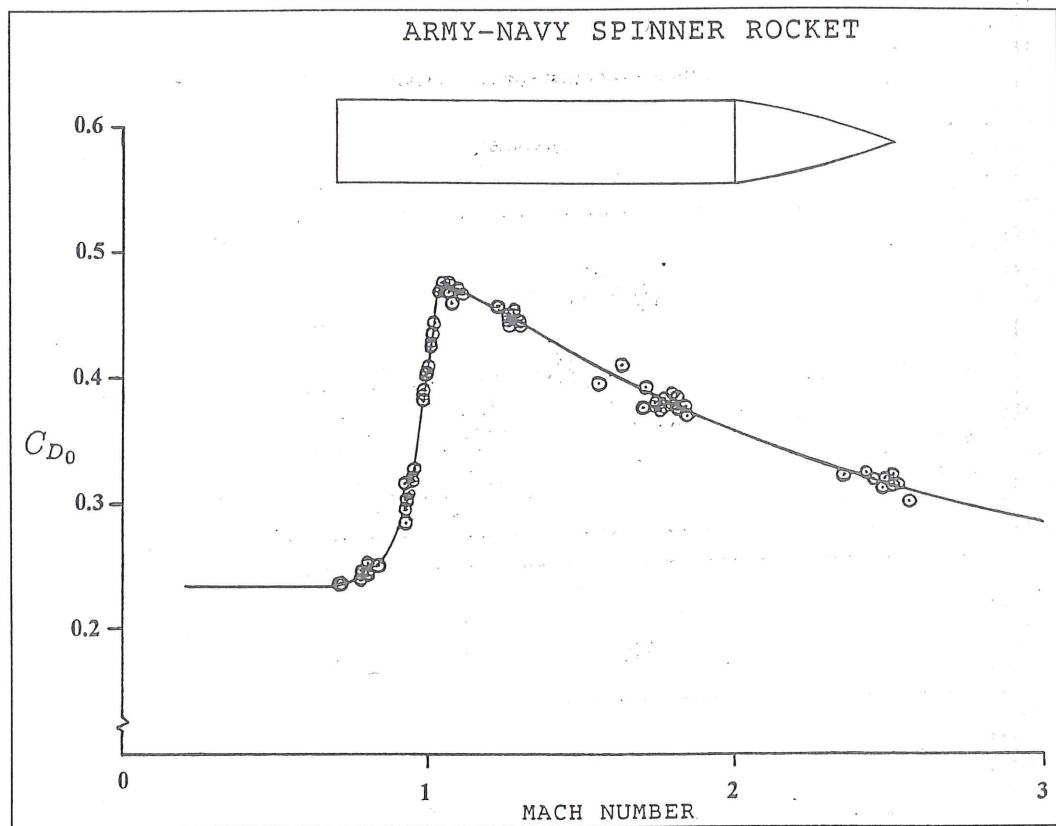


Figure
Coeffici

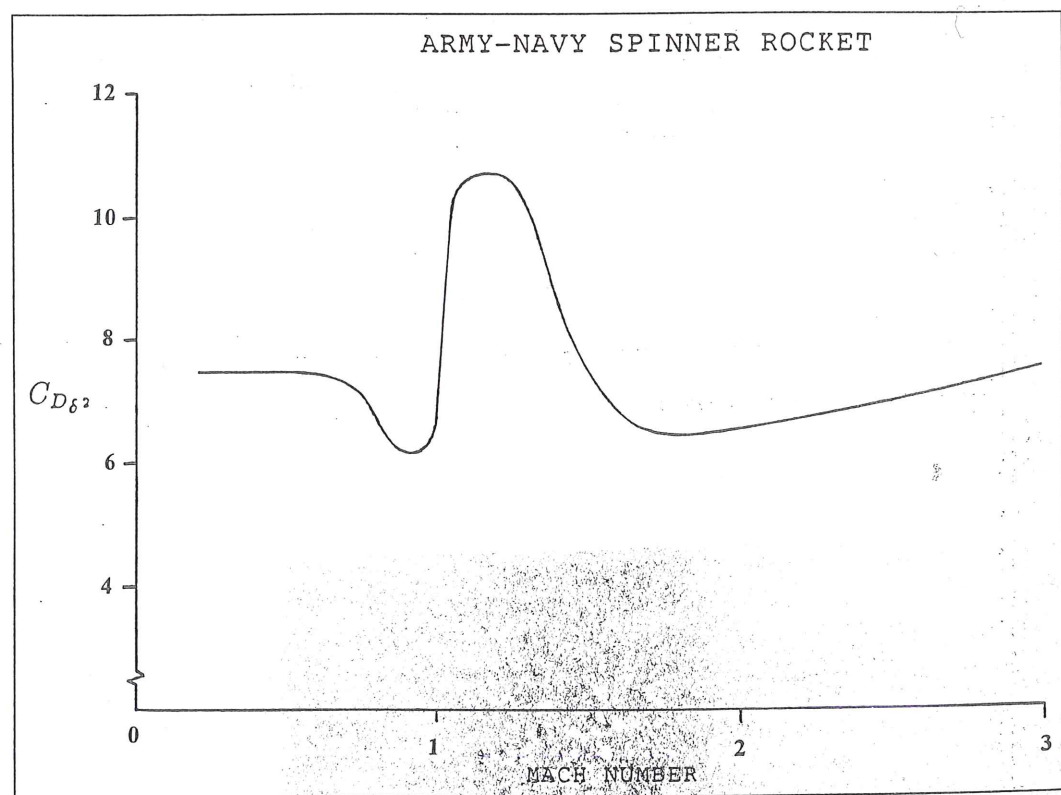


Figure
Coeffici

Measurement of Aerodynamic Forces and Moments

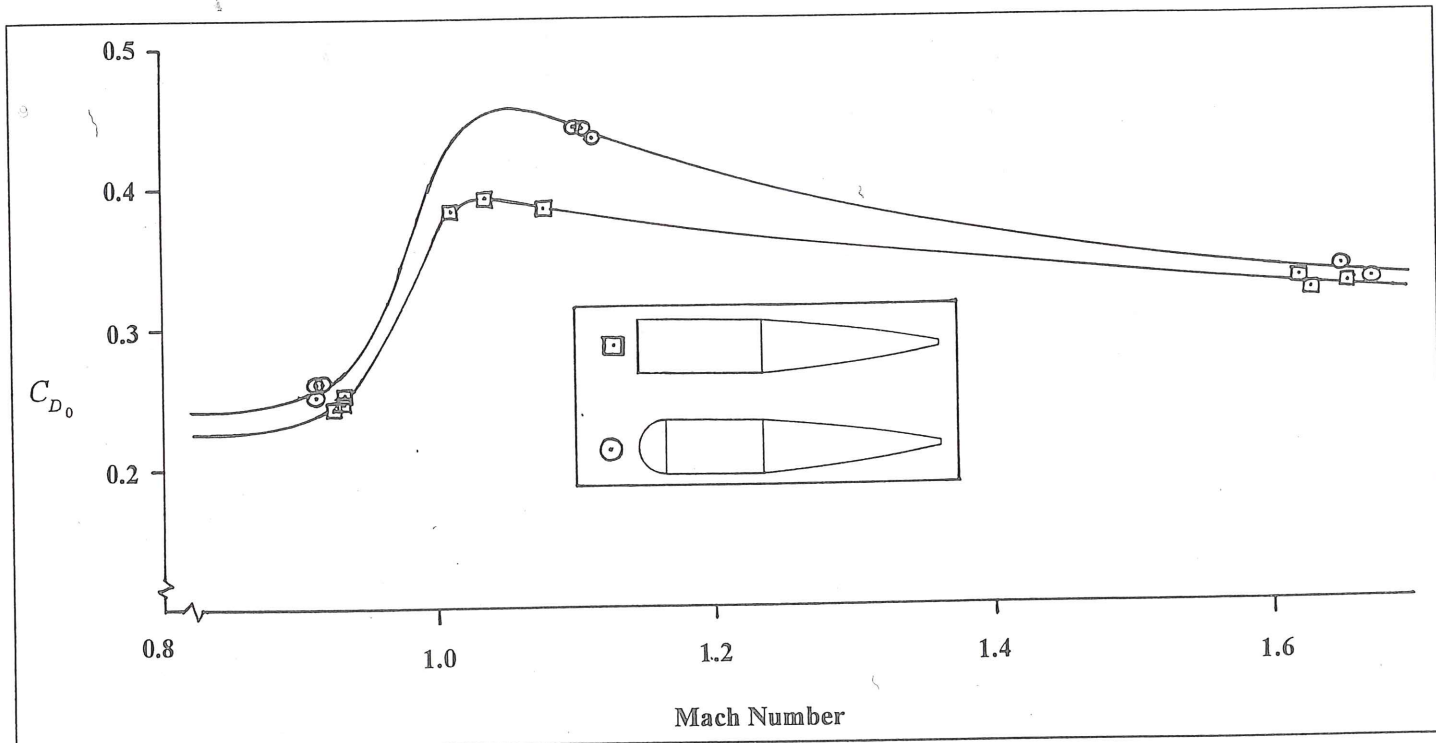


Figure 14.16 Zero-Yaw Drag Coefficient vs. Mach Number.

spherical base effectively shifts the normal force center-of-pressure farther toward the tail of the projectile, relative to the flat-based model. This effect is caused by the difference in the boundary layer separation point on the windward and leeward sides of the hemisphere.

Figure 14.18 (p. 318) illustrates the behavior of the Magnus moment coefficient and the pitch damping moment coefficient for the flat-based and the hemispherical-based shell. This figure clearly shows the reason for the observed poor flight characteristics of hemispherical-based projectiles. The upper plot of Figure 14.18 shows that the hemispherical based models have large negative Magnus moment coefficients at all flight speeds, and this condition alone is sufficient to cause slow-arm dynamic instability. In addition, the lower plot shows that the pitch damping moment coefficient for a hemispherical-based shell is positive at all speeds! The unfortunate combination of a large negative Magnus moment coefficient *and* a positive pitch damping moment coefficient produces a strong slow-arm dynamic instability. Projectile designers should therefore avoid hemispherical-based shell designs whenever possible.

14.5 SIX-DEGREES-OF-FREEDOM DATA REDUCTION FOR SPARK RANGES

The Chapman-Kirk 6-DOF data reduction method was first advanced in 1969, in a paper (Ref. 26) presented at the AIAA (American

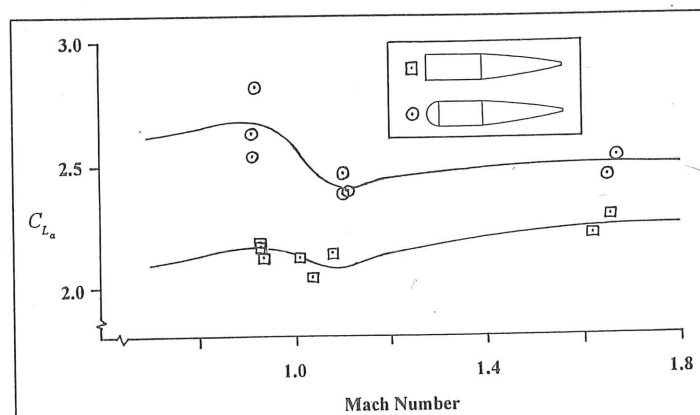


Figure 14.17(a). Lift Force Coefficient vs. Mach Number

